

# Death rate of massive stars at redshift $\sim 0.3$ \*

E. Cappellaro<sup>1</sup>, M. Riello<sup>2,3,4</sup>, G. Altavilla<sup>5</sup>, M. T. Botticella<sup>1,6</sup>  
S. Benetti<sup>3</sup>, A. Clocchiatti<sup>7</sup>, J. I. Danziger<sup>8</sup>, P. Mazzali<sup>8</sup>, A. Pastorello<sup>9</sup>, F. Patat<sup>2</sup>, M. Salvo<sup>10</sup>  
M. Turatto<sup>3</sup>, S. Valenti<sup>1,11</sup>

<sup>1</sup> INAF - Osservatorio Astronomico di Capodimonte, Salita Moiariello, 16, I-80131, Napoli, Italy  
e-mail: [cappellaro@na.astro.it](mailto:cappellaro@na.astro.it)

<sup>2</sup> European Southern Observatory, K. Schwarzschild Str. 2, 85748 Garching, Germany

<sup>3</sup> INAF - Osservatorio Astronomico di Padova, Vicolo dell'Osservatorio, 5, I-35122, Padova, Italy

<sup>4</sup> Dipartimento di Astronomia - Università di Padova, Vicolo dell'Osservatorio, 2, I-35122, Padova, Italy

<sup>5</sup> Departament d'Astronomia i Meteorologia, Universitat de Barcelona, Martí i Franqués 1, 08028 Barcelona, Spain",

<sup>6</sup> Osservatorio Astronomico di Collurania, via M. Maggini, I-64100 Teramo, Italy Dipartimento di Scienze della Comunicazione, Università di Teramo, viale Crucoli 122, I-64100 Teramo, Italy

<sup>7</sup> Departamento de Astronomía y Astrofísica, Pontificia Universidad Católica, Chile

<sup>8</sup> INAF - Osservatorio Astronomico di Trieste, via Tiepolo, 11, I-34131, Trieste, Italy

<sup>9</sup> INAF - Osservatorio Astronomico di Arcetri, Largo E. Fermi 5, I-50125 Firenze, Italy

<sup>10</sup> Australian National University, Mount Stromlo Observatory, Cotter Road, Weston ACT 2611, Australia

<sup>11</sup> Dipartimento di Fisica - Università di Ferrara, via del Paradiso 12, I-44100 Ferrara, Italy

Received .../ Accepted ...

**Abstract.** We report the first result of a supernova search program designed to measure the evolution of the supernova rate with redshift. To make the comparison with local rates more significant we copied, as much as possible, the same computation recipes as for the measurements of local rates. Moreover, we exploited the multicolor images and the photometric redshift technique to characterize the galaxy sample and accurately estimate the detection efficiency.

Combining our data with the recently published measurements of the SN Ia rate at different redshifts, we derived the first, direct measurement of the core collapse supernova rate at  $z = 0.26$  as  $r_{cc} = 1.45_{-0.45}^{+0.55} h^2 \text{ SNU}$  [ $h=H_0/75$ ]. This is a factor three ( $\pm 50\%$ ) larger than the local estimate. The increase for a look back time of "only" 2.8 Gyr is more rapid than predicted by most of the published models of the SN rate evolution. Core-collapse SN rates measure the death rate of massive star and, because of the short time scale of evolution, can be translated in a measurement of the ongoing SFR. Assuming a Salpeter IMF and the standard scenario for core-collapse progenitors we derived to an estimate of the star formation rate at redshift  $3.1_{-1.0}^{+1.1} \times 10^{-2} h^3 M_{\odot} \text{ yr}^{-1} \text{ Mpc}^{-3}$  which compare very well with a recent estimate based on the measurement of the  $H\alpha$  luminosity density at the same redshift.

**Key words.** supernovae:general – star:formation – galaxy:evolution – galaxy:stellar content

## 1. Introduction

Supernova rates represent a link between the evolution of individual stars and that of stellar systems. In particular, the rate of type II + Ib/c SNe measures the death rate for core-collapse (CC) of young, massive stars and, because of the short time-scale of the progenitor evolution (Heger et al. 2003), directly reflects the on-going star for-

mation rate (SFR) in a given environment. On the contrary, the rate of type Ia SNe, which result from long-lived, low mass binary systems (Branch et al. 1995) reflects the long-term star formation history. Owing to the very high intrinsic luminosity, SNe can be seen at very large distances and hence measurements of SN rate evolution with redshift can be used to trace the history of the SFR with cosmic age.

Studies of the evolution of SN rates with redshift are now strongly unbalanced towards theory. In recent years, many authors have published predictions of the SN rate as a function of redshift based on the SN progenitor scenar-

Send offprint requests to: E. Cappellaro, e-mail: [cappellaro@na.astro.it](mailto:cappellaro@na.astro.it)

\* Based on observations collected at the European Southern Observatory, Chile (ESO Programmes 62.H-0833, 63.H-0322, 64.H-0390, 67.D-0422, 68.D-0273, 69.D-0453).

ios and the modeling of the cosmic star formation history (Madau, Della Valle, & Panagia 1998; Sadat et al. 1998; Dahlnén & Fransson 1999; Yungelson & Livio 2000; Kobayashi, Tsujimoto, & Nomoto 2000; Sullivan et al. 2000; Calura & Matteucci 2003). Despite the strong interest, observational estimates of the SN rate at high redshift are still very scanty. The few published measurements are based on SN searches aimed at using type Ia SNe as cosmological probes (Pain et al. 1996; 2002; Tonry et al. 2003) and, as a consequence, they are strongly biased towards type Ia. To date, there is no direct measurement of the evolution of core-collapse SN rates.

With the goal to fill this gap, we initiated a long term project aimed to measure the rate evolution with redshift for all SN types. In this paper we report the first results of this effort, namely an estimate of the core-collapse SN rate at redshift  $z \sim 0.3$ .

To reduce the systematics in the comparison with the local rate, our strategy we followed as closely as possible the same approach used in that context (Cappellaro et al. 1997; Cappellaro, Evans, & Turatto 1999). The process consists of four steps: *i*) SN candidate detection and, when possible, spectroscopic classification (Sec. 2); *ii*) characterization of the galaxy sample through galaxy photometric redshifts; estimate of distances and calibration of the absolute luminosities for each galaxy (Sec. 3); *iii*) evaluation of the SN detection efficiency and thus of the effective surveillance time for each galaxy of the sample (Sec. 4); *iv*) estimate of the SN rate per unit luminosity. To round up the paper, we discuss the main sources of uncertainty (Sec. 6) and discuss the implication of our results (Sec. 7).

## 2. The supernova search

The building block of a SN search is the detection of variable sources through the comparison of images of selected sky fields obtained at different epochs. In general, the temporal sampling of the observations is tuned to the specific goal one wants to achieve. For the use of type Ia as cosmological distance indicators it is crucial to catch SNe as early as possible and hence, accounting for the typical rise time, the observations have to be spaced by 2-3 weeks. Instead, to maximize the event statistics, the time elapsed between exposures should be equal (or longer) than the time a typical event remains brighter than the search detection limit. The latter, of course, depends on the target distance (or redshift) and the SN type. **Independently on the temporal sampling, to ensure that all SNe are detected, the time elapsed between the first and the last observation of a given field have to be longer that time for a significant luminosity evolution for all SN type. The latter can be as long as 3-4 months for SN IIP and even longer for type IIc.**

For our search we selected 21 fields, evenly distributed in right ascension, which have been monitored for about 2 years with an average sampling of one observation every three months. However, the results reported in this paper

are based on observations of 5 fields only, i.e. those with the best temporal and filter coverage. The full sample will be presented in a future paper (Riello et al. 2004, in preparation). **The observing log is shown in Tab. 1. For each field we give the center coordinates and, for the epochs when observations are available, we list the seeing.**

A typical observing run was splitted into two parts: the search and the follow-up observation of candidates.

For the search, two consecutive nights were devoted at the ESO/MPI 2.2m telescope at ESO, La Silla (Chile). The telescope was equipped with the Wide Field Imager (WFI) and a mosaic of  $2 \times 4$  CCD detectors of  $2048 \times 4096$  pixels which image a sky area of  $\sim 0.25 \text{ deg}^2$  with an excellent spatial resolution of  $0.238 \text{ arcsec/pix}$ .

**When possible**, the first observing night was dedicated to obtain deep  $V$  band exposures for candidate detection while in the second night the same fields were observed through a different filter,  $B$  or  $R$ , with the purpose of collecting color information both for the candidates and the galaxies. **Unfortunately, due to a number of technical, meteorological and scheduling constraints in many cases we could not maintain this observing strategy as can be seen from Tab. 1. This implies that only in a few cases we could derive the candidate color. For homogeneity, in the following statistical computation we considered only the candidates detected in the  $V$  band exposures.**

In order to get rid of detector cosmetic defects, cosmic rays, satellite tracks and fast moving objects, for each field we obtained three 900 s exposures dithered by 5-10 arcsec.

Follow-up observations were scheduled about one week after the search at the VLT+FORs1/2 at ESO Paranal for the spectroscopic classification of some of the candidates. The VLT was needed, as most of our SN candidates are in the magnitude range  $V \simeq 22.5\text{--}23.5 \text{ mag}$ . For a proper subtraction of the night sky emissions we selected grisms of moderate resolution, namely grism 300V and/or 300I (resolution  $\sim 10\text{\AA}$  FWHM), which allowed us to cover a quite wide wavelength range ( $4000 \div 11000\text{\AA}$ ). Depending on the candidate magnitude, exposure times ranged from 900s to 3 hours. Details on the reduction of the spectroscopic observations and of the spectral analysis will be given elsewhere. Here we make use only of the spectral classification and redshift.

The analysis of the search images began with the removal of the instrument signature and calibration for which we used IRAF<sup>1</sup> and *MSCRED*, a package specifically designed to handle mosaic images (Valdes 1998). Indeed, after bias subtraction and flat fielding, the individual dithered exposures were astrometrically calibrated and stacked in a single image. For photometric nights, observations of standard fields were used for absolute cal-

<sup>1</sup> IRAF is distributed by the National Optical Astronomy Observatories, which are operated by the Association of Universities for Research in Astronomy, Inc., under cooperative agreement with the National Science Foundation.

**Table 1.** Observing log of the SN search fields. For each field, when observations in a given band are available, we report the measure of the seeing in arcsec (FWHM on the stellar objects on the combined image)

field	J1888			AXAF			10Z2			13Z3			Field2		
R.A. (2000.0)	00h 57m 35.4s			03h 32m 23.7s			10h 46m 45.8s			13h 44m 28.3s			19h 12m 51.9s		
Dec.	−27d 39m 16s			−27d 55m 52s			−00d 10m 03s			−00d 07m 47s			−64d 16m 31s		
run	B	V	R	B	V	R	B	V	R	B	V	R	B	V	R
1999/02/23							1.1			1.1					
1999/03/10							1.1	1.3		1.2	1.2				
1999/03/19							1.0	0.9		1.0	0.8				
1999/05/08							1.3	1.4		1.4			1.9	1.6	1.0
1999/05/17							0.8	0.9	1.0	1.7	1.0	0.9	0.7	0.8	
1999/08/03	1.0	1.4	1.3							1.4			1.1	1.8	
1999/09/13	1.6	1.4	1.2		1.2									1.7	
1999/11/09	1.0	0.8		1.1	1.0										
1999/12/02		1.0		1.0	1.1										
1999/12/10		1.7						1.3							
1999/12/28		1.9			1.2										
2000/11/16		1.0			0.9										
2000/12/17		1.0			0.9										
2001/04/18								1.0			0.9			0.8	
2001/11/11-12		0.7	1.2		1.0	0.9									
2001/11/18		1.0			0.8										
2001/12/08-09		0.9	0.8		1.0	0.8									
2002/04/07-08							1.9	0.9		0.8	1.1		1.3	1.3	

ibration (Landolt 1992). Otherwise, the photometric zero point was established by comparison with a calibrated image of the same field.

For each field we computed the difference between the image to be searched (target image) and a suitable archive frame (template image). Indeed, after accurate astrometric and photometric registrations, the most crucial step in this process is the matching of the point spread function (PSF) of the two images. This was done using the *ISIS2.1* package (Alard 2000) that, from the comparison of the same sources in the two images, computes a space-varying convolution kernel to degrade the image with the best seeing to match the other one. Taking into account that the best subtraction is obtained when the two images have similar PSFs, and that we want to preserve as much as possible the resolution of the target image, we had to maintain an archive with template images with different seeing. Populating the archive required a significant investment of telescope time and this was the reason why the search became really efficient only after some time from the first observations.

Variable sources leave residuals in the difference image which have been detected and logged into a catalogue using the *SExtractor* program (Bertin & Arnouts 1996) which has also the capability of separating stars from galaxies. Due to residuals of poorly removed bright stars or cosmic rays, the variable source catalogue contains many false detections, most of which are quickly eliminated by means of a custom made ranking program. This makes use of information from the difference image as well as from the target and template images and it has been tuned through extensive artificial stars experiments. The surviving candidates, typically a few tens per field, are all

checked visually by a human expert. Among these, a few are still obvious false detections which could not be properly flagged by our software but are quickly eliminated by visual inspection. Among these are residuals of moving objects which are not completely masked by our dithering strategy. After that, we are left with true variable source among which we remove variable stars, objects with stellar profile present both in the target and template image, but with different magnitudes. At the end of this process, one is left with the fiduciary SN candidates, typically from none to a handful per field.

Ideally, one would need spectroscopic confirmation for all the candidates. Unfortunately, because of the limited VLT time available, we could obtain spectroscopic observations for  $\sim 20\%$  of the detected SN candidates only. This is the main weakness of the work presented here. On the other hand, we could verify the reliability of our SN candidate selection criteria: out of the 29 candidates for which we have obtained VLT spectra during the entire search project, 22 turned out to be SNe (45% type Ia and the other type II and Ib/c) and 7 variable AGNs. We stress that our approach to candidate selection was designed to avoid as much as possible any selection bias and in particular, we do not exclude a priori nuclear candidates. Given that, the intrusion of AGNs is unavoidable.

Even without spectroscopy, contamination by variable AGNs can be reduced by looking at the long term variability history of the candidates. With this aim we kept a database, powered by *MySQL*<sup>2</sup>, which is used to search

<sup>2</sup> MySQL is an open source database without a license fee under the GNU General Public License (GPL). See the project homepage for further details. <http://www.mysql.com/>

**Table 2.** SN candidates of the fields of Tab. 1

designation	R.A.			Dec.			V mag		offset arcsec	z phot.	n. exp.	first detect.	search class.
	2000.0			cand.	host								
J1888-H	00h 56m 26.25s	-27d 43m 31.8s	22.9	20.0	0.4	0.19	3	00/11/16	SN				
J1888-F	00h 56m 26.89s	-27d 27m 56.5s	22.5	16.1	0.4	0.20	6	99/11/09	SNAGN				
J1888-D	00h 56m 31.54s	-27d 31m 17.2s	23.5	21.1	0.4	0.30	6	01/11/11	SN				
J1888-C	00h 56m 33.40s	-27d 52m 52.3s	21.9	21.5	0.2	0.42	9	99/12/10	SN				
J1888-L	00h 56m 38.43s	-27d 45m 07.9s	23.4	20.1	0.1	0.32	3	99/11/09	SNAGN				
SN2001gh	00h 57m 03.63s	-27d 42m 32.9s	20.8	22.2	0.4	0.27	15	01/12/08	SN spec				
J1888-M	00h 57m 05.34s	-27d 45m 57.7s	23.4	21.8	0.2	0.19	3	01/12/08	SNAGN				
J1888-G	00h 57m 29.24s	-27d 40m 56.3s	22.6	19.0	0.2	0.17	3	99/12/10	SNAGN				
J1888-B	00h 57m 48.08s	-27d 54m 13.3s	21.0	21.8	0.1	0.56	15	99/08/03	SN				
J1888-Q	00h 57m 51.11s	-27d 51m 28.3s	23.8	22.0	0.5	0.18	3	99/11/09	SN				
J1888-N	00h 58m 01.76s	-27d 53m 15.5s	23.5	21.0	<0.1	0.32	6	99/11/09	SNAGN				
SN1999ey	00h 58m 03.42s	-27d 40m 31.2s	20.2	21.3	1.1	0.01	15	99/11/09	SN spec				
J1888-K	00h 58m 33.21s	-27d 27m 56.9s	23.3	20.5	0.2	0.31	3	99/12/02	SNAGN				
SN2000fc	00h 58m 33.55s	-27d 46m 40.1s	22.5	22.6	0.4	0.33	6	00/11/16	SN spec				
J1888-J	00h 58m 41.36s	-27d 50m 38.1s	22.9	20.7	0.6	0.38	3	99/11/09	SN				
SN2001ip	03h 31m 13.03s	-27d 50m 55.5s	23.5	21.8	0.1	0.39	6	01/12/08	SN spec				
AXAF-E	03h 31m 17.11s	-28d 04m 47.9s	23.3	21.8	0.1	0.24	3	00/12/17	SNAGN				
AXAF-A	03h 31m 28.46s	-28d 07m 57.4s	23.0	22.6	0.3	-	3	99/12/28	SN				
AXAF-D	03h 31m 28.98s	-28d 10m 26.1s	23.4	22.8	0.2	0.52	6	99/12/28	SN				
AXAF-J	03h 31m 39.12s	-27d 53m 00.5s	23.7	18.9	0.2	0.14	3	00/12/17	SNAGN				
AXAF-H	03h 31m 49.98s	-28d 09m 41.6s	23.6	22.7	0.4	-	3	91/12/08	SN				
AXAF-I	03h 32m 11.18s	-28d 03m 49.6s	23.7	20.3	0.2	0.15	3	01/12/08	SNAGN				
SN1999gt	03h 32m 11.57s	-28d 06m 16.2s	22.0	20.8	2.2	0.17	3	99/12/28	SN spec				
AXAF-B	03h 32m 31.16s	-28d 04m 43.9s	22.7	18.9	0.4	0.17	3	99/12/28	SN				
AXAF-C	03h 32m 45.62s	-28d 08m 41.7s	23.8	20.2	0.1	0.22	3	99/12/28	SNAGN				
SN1999gu	03h 33m 00.22s	-27d 51m 42.7s	21.6	18.9	2.6	0.15	3	99/12/28	SN spec				
AXAF-F	03h 33m 05.30s	-27d 54m 09.2s	23.2	21.8	0.2	0.26	3	99/12/02	SN				
SN2002cl	13h 44m 09.94s	-00d 12m 57.8s	21.6	16.5	3.0	0.07	6	02/04/07	SN spec				
10Z2-B	10h 45m 42.76s	+00d 00m 28.0s	22.8	21.7	0.5	0.10	6	02/04/07	SN				
10Z2-A	10h 47m 06.52s	+00d 00m 39.7s	21.9	21.1	0.3	0.69	6	02/04/08	SN				
10Z2-D	10h 47m 40.94s	-00d 13m 52.7	23.4	21.5	0.6	0.76	6	99/03/19	SN				
13Z3-A	13h 43m 28.86s	-00d 14m 22.1s	23.8	21.9	0.5	0.39	6	02/04/06	SN				
13Z3-D	13h 43m 42.41s	+00d 06m 44.9s	23.2	20.9	0.2	0.46	6	99/03/10	SNAGN				
13Z3-I	13h 44m 18.49s	-00d 20m 55.5s	23.7	21.8	< 0.1	0.13	3	99/03/19	SNAGN				
13Z3-K	13h 45m 07.50s	+00d 04m 06.9s	23.4	20.1	0.2	-	9	99/03/10	AGN spec				
13Z3-C	13h 45m 26.39s	-00d 18m 10.6s	23.1	19.8	0.7	0.15	3	01/04/18	SN				
13Z3-H	13h 45m 26.95s	+00d 08m 04.0s	23.5	20.7	0.3	0.28	3	99/05/17	SN				
SN2001bd	19h 13m 10.94s	-64d 17m 07.8s	21.7	16.8	3.5	0.15	3	01/04/18	SN spec				
Field2-F	19h 14m 01.64s	-64d 22m 38.6s	22.7	22.0	0.8	0.33	3	01/04/18	SN				
Field2-G	19h 14m 51.24s	-64d 19m 34.9s	22.9	20.9	<0.1	0.07	3	01/04/18	SNAGN				

for multiple detections of the same source (Riello 2003). If the source shows long-term, erratic variability, it is excluded from the list of SN candidates. For the candidates which passed this selection and that were centered on the host galaxy nucleus ( $\sim 30\%$ ) we found that 40% were actually SNe while the remaining ones were still AGNs. To take this into account, in all the calculations nuclear candidates were given a statistical weight of 0.4. Note that with the progressing of the monitoring, AGN contamination will continue to be reduced.

In the 5 fields discussed in this paper, we have detected 40 candidates. **These are listed in Tab.2 where we report the candidate designation (col. 1), coordinates (cols. 2-3), and apparent V magnitude at discovery (col. 4), the apparent V magnitude of**

**the host galaxy (col. 5), the offset (in arcsec) from the host nucleus (col. 6), the host photometric redshift (col. 7), the number of individual exposures in which the object has been seen (col. 8) and the epoch of first detection (col. 9). In the last column we report the classification of the candidate. Candidates located in the host galaxy nuclear regions are labelled SNAGN and are given a smaller weight as described above.**

For 9 of the candidate we obtained spectroscopic observations which were used to derive spectral classification and redshift (Tab. 3). Eight of these objects were confirmed as SNe, classified as type Ia (3), type II (4) and type Ic (1). One object was found to be a Seyfert 1 galaxy.

**Table 3.** SN candidates with spectroscopic classification

Designation	Type	Redshift	Field	Reference
SN1999ey	IIn	0.094	J1888	IAUC 7310
SN1999gt	Ia	0.275	AXAF	IAUC 7346
SN1999gu	II	0.149	AXAF	IAUC 7346
SN2000fc	Ia	0.430	J1888	IAUC 7537
SN2001bd	II-L	0.096	Field2	IAUC 7615
SN2001gh	II-P	0.159	J1888	IAUC 7762
SN2001ip	Ia	0.536	AXAF	IAUC 7780
SN2002cl	Ic	0.072	13Z3	IAUC 7785
13Z3-K	Sy1	0.362	13Z3	–

### 3. The Galaxy Sample

The estimate of SN rates in the local Universe relies on the characterization of the galaxy sample which have been searched (Cappellaro et al. 1997). For each galaxy one needs to know the distance, which enters the computation of the surveillance time, and the integrated luminosity, which is used as a normalization factor. Indeed, it has been demonstrated that the SN rate scales with the size of the parent stellar population as measured from the integrated blue luminosity (Cappellaro et al. 1993). For nearby galaxies the relevant information can be readily retrieved from published catalogues, while this is not the case when one goes to larger distances.

In an attempt to follow the same approach for our intermediate redshift SN project, we exploited the  $B$ ,  $V$ ,  $R$  images obtained during the search to measure magnitudes and colors of the galaxies detected in our fields and we used them to derive distances and absolute luminosities through the SED fitting photometric redshift technique (Bolzonella et al. 2000).

With this aim we selected from the image archive, for each field and band, the exposures obtained under the best conditions, in particular those with seeing  $< 1''$ , which were stacked together using the *SWARP* package by E. Bertin (cf. <http://terapix.iap.fr/>). This produces a sensible gain in the  $S/N$  ratio: while the limiting magnitude of a typical search image is  $V \sim 24.5$ , the same for the stacked image is  $V \sim 26$  ( $3 - \sigma$  point source).

From the  $V$  images, which compared to the other bands benefit from longer cumulative exposure times, we built the galaxy catalogue including all sources with *SExtractor* stellarity index  $\leq 0.9$  (Arnouts et al. 2001). A further selection is performed excluding galaxies fainter than  $R = 21.8$ . While this limit was originally chosen to improve our confidence in the photometric redshifts (see next), it has also the advantage that up to this magnitude the  $S/N$  is good enough to guarantee a clean star-galaxy separation and a good photometric accuracy. For these selected galaxies,  $B$  and  $R$  magnitudes were eventually measured adopting the same aperture as defined in the  $V$  image.

Photometric redshifts were estimated using the *hyper-z* code (Bolzonella et al. 2000). This program searches for

the best match between the measured colors of galaxies and the values in a grid created from a library of spectral energy distribution (SED) templates for different redshifts. It has been shown that with a proper sampling of the SED, even with broad band filters, galaxy redshifts can be measured with an RMS error as small as  $\sigma \sim 0.05$  (Bolzonella et al. 2000). In our case, however, with observations in only three bands we cannot match this level of accuracy. In particular, we note that one of the most significant features in the galaxy SED, the 4000Å break, falls redward of the  $R$  band for redshifts larger than  $z > 0.8$ . This means that the redshifts derived for more distant galaxies are very uncertain.

On the other side we notice that, because of the observing strategy and limiting magnitude, the SNe discovered in our search are all at  $z < 0.8$  with a peak of the distribution at  $z \sim 0.3$ . To remove as much as possible the contamination of distant galaxies erroneously estimated at low redshift, we removed from the sample galaxies fainter than  $R = 21.8$ . This roughly corresponds to the magnitude  $M_*$  at a redshift  $z = 0.8$  (Wolf et al. 2003), where  $M_*$  is a parameter of the Schechter function (Schechter 1976) which is used to fit the galaxy luminosity function. With this choice, galaxies with redshift  $\geq 0.8$  contribute about 20% of the total sample luminosity.

At the same time, low luminosity galaxies at low redshift are removed from the sample. However at  $z \sim 0.3$ , the average redshift of our search, they contribute to only 1/4 of the total luminosity and they are expected to give a small contribution to the SN productivity. Indeed we found that out of the 40 SN candidates, only 2 (**AXAF-H** and **AFAX-A**, which were not included in the computations) were discovered in galaxies fainter than  $R = 21.8$ .

The final galaxy catalog, which counts about 11300 galaxies, was cross-checked with NED in order to assess the accuracy of the photometric redshifts. We found that spectroscopic redshifts were available for 324 galaxies (including 118 galaxies of the field J1888 for which spectroscopic redshift were kindly provided by P.-A. Duc, in advance of publication). With these data we built the histogram of  $\Delta z = (z_{\text{ph}} - z_{\text{sp}})/(1 + z_{\text{sp}})$ , the differences between spectroscopic and photometric redshifts, which is shown in Fig. 1 (dashed line). It turns out that the average difference is  $\langle \Delta z \rangle = 0.01$  with a RMS error  $\sigma = 0.10$ , which is both consistent with our limited SED sampling and sufficient for our statistical analysis. An independent check on the accuracy of our photometric redshift was made possible by the fact that one of our fields (AXAF) partially overlaps with the Chandra Deep Field South covered by the COMBO-17 survey (Wolf et al. 2003). The distribution of  $\Delta z$  for 1375 galaxies which we have in common is also shown in Fig 1 (thick line). The average difference  $\langle \Delta z \rangle = 0.00$  with a RMS error  $\sigma = 0.11$  is very similar to those measured in the comparison with spectroscopic redshifts.

The redshift distribution of our galaxy sample is shown in Fig. 2. As expected, given the adopted limiting magnitude, the number counts peak at about  $z \sim 0.3$ . For

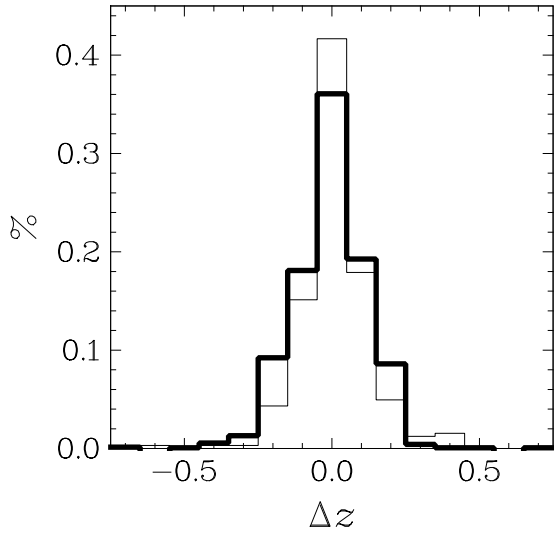


**Fig. 1.** Distribution of  $\Delta z = (z_{ph} - z_{sp})/(1 + z_{sp})$ , the difference between our estimate of the photometric redshift and *a)* spectroscopic redshifts, for the 324 galaxies of our sample with known spectroscopic redshift (thin line) and *b)* COMBO17 photometric redshifts Wolf et al. (2003) for the 1375 galaxies which are in common with our sample (thick line)

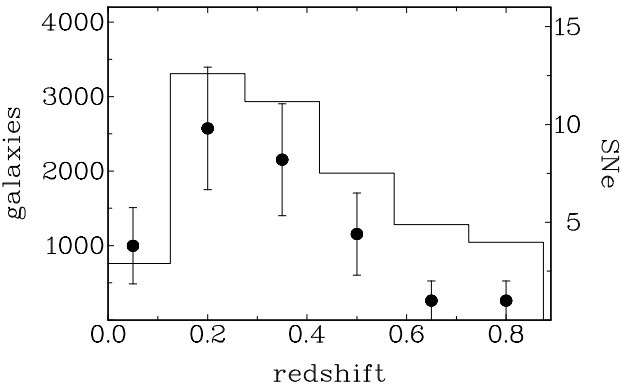


**Fig. 2.** Redshift distribution of our galaxy sample (line, left-side scale) and SNe host galaxies (dots, right-side scale). For the latter, candidates coincident with the host galaxy nucleus have been counted with a 0.4 weight.

comparison, in Fig. 2 we have also plotted the redshift distribution of the SN candidate host galaxies (dots) with their statistical errors.

#### 4. Detection Efficiencies and Control Time

The computation of rates requires the definition of the time interval during which the events could be detected.

We need to estimate the time during which a SN hosted in a given galaxy remains brighter than the search detection threshold which is usually referred to as *control time*. This depends on *i)* the search threshold and detection efficiency; *ii)* the SN absolute magnitude and luminosity evolution, *iii)* the distance.

There are several concurrent factors determining the detection efficiency. For a given instrument and fixed exposure time, the key factors are the observing conditions, in particular sky transparency and seeing. There is also some dependence on the characteristics of the particular sky field, due to the disturbing presence of bright stars and nearby galaxies. The position of the candidate within the parent galaxy plays also a role.

While the sky transparency of a specific observation is measured by the photometric constants, the impact of other factors was evaluated performing a number of artificial star experiments. In these simulations we placed a number of synthetic stars with a given magnitude  $m$ , and the PSF deduced from field stars, distributing them in different galaxies of the field. The position of the artificial stars within the host galaxy was chosen randomly, assuming a gaussian distribution centered on the galaxy nucleus and a FWHM equal to that of the host galaxy. Then, the synthetic frames were processed through our search pipeline and the detection efficiency  $\epsilon(m)$  was computed as the ratio between recovered and injected stars.

In Fig. 3 we plot an example of detection efficiency function for one of the observation of the field AXAF. As a result of these numerical experiments, which will be described in detail in a forthcoming paper (Riello et al. 2004), we found that the most critical parameter is the seeing. In particular we found that, taking as reference the magnitude at which the detection efficiency is 50%, this is  $\sim 1.2$  mag fainter when the seeing is  $0''.65$  compared with a seeing of  $1''.3$ .

The other factor entering the computation of the control time for a given epoch is the SN luminosity evolution and its absolute luminosity. The prescription we used in our calculations is described in the following. The apparent  $V$  light curve for each SN was computed taking into account the luminosity distance (estimated from the photometric redshift of the host galaxy), the time dilation and the  $K$ -correction according to the following relation:

$$m_{i,V}^{\text{SN}}(t) = M_B^{\text{SN}}(t_0) + \mu(z_i) + K_{BV}^{\text{SN}}(t_0) + A_V^G \quad (1)$$

where, for the  $i$ -th galaxy at redshift  $z_i$ ,  $t_0 = t/(1 + z_i)$  is the galaxy rest frame time,  $M_B^{\text{SN}}(t_0)$  is the SN light curve in  $B$  absolute magnitude,  $\mu(z_i)$  is the galaxy distance modulus<sup>3</sup>,  $K_{BV}^{\text{SN}}(t_0)$  is the  $B$  to  $V$   $K$ -correction and  $A_V^G$  is the galactic extinction in  $V$  (the superscript  $SN$  indicates SN type dependent quantities).

Following Cappellaro et al. (1997), we considered four basic SN types, namely Ia, IIP, IIL and Ib/c. Guided by the general theoretical interpretation, type IIP, IIL, and

<sup>3</sup> Hereafter, we assume a standard flat cosmology  $\Omega_M = 0.3$  and  $\Omega_\Lambda = 0.7$  and  $h = H_0/75$

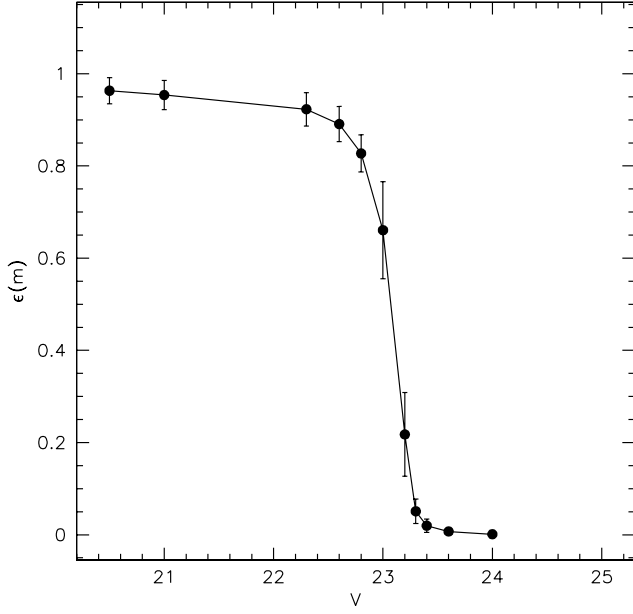


**Fig. 3.** Example of SN detection efficiency curve, plotted as a function of apparent magnitude for one of the epochs of field AXAF (seeing 0'9).

Ib/c will be collectively called later *core collapse* (CC) SNe.  $B$  absolute magnitudes and light curves were also taken as in Cappellaro et al. (1997). The  $K_{BV}^{\text{SN}}$ -correction for each SN type at different phases was calculated using a sample of spectra with good  $S/N$  ratio available in the Asiago-Padova SN archive. Spectra were redshifted by the proper amount and synthetic photometry was computed using the *synphot* package in *IRAF*. The choice of the  $K_{BV}$  correction is motivated by the fact that, for the average redshift of our search,  $\langle z \rangle \sim 0.3$ , this minimizes both the uncertainties and the time dependence of the  $K$ -correction. Note that for the same reason we use as reference  $B$  light curves of local SNe.

We introduce here the effective control time defined, for each observation of a given galaxy, as the control time weighted by the galaxy luminosity in units of  $10^{10}L_{B\odot}$ :

$$CT_i^{\text{SN}} = L_i \int \tau_i^{\text{SN}}(m) \epsilon(m) dm \quad (2)$$

where  $\tau_i^{\text{SN}}(m)$  is the time a SN in the  $i$ -galaxy stays at a magnitude between  $m$  and  $m+dm$ , and can be computed from relation (1),  $\epsilon(m)$  is the detection efficiency at the given magnitude and  $L_i$  is the luminosity of the  $i$ -th galaxy in units of  $10^{10}$  blue-band solar luminosities.

Finally, for the given galaxy the total control time of the search campaign,  $\overline{CT}_i^{\text{SN}}$ , is obtained by properly combining the control time of individual observations (cf. Cappellaro et al. 1999).

## 5. SN Rates

For a given galaxy and SN type, the rates are derived by dividing the number of observed events by the total control time:

$$r_i^{\text{SN}} = (1 + z_i) \frac{N^{\text{SN}}}{\overline{CT}_i^{\text{SN}}} \quad (3)$$

where the factor  $1 + z$  corrects the rate to the rest frame.

The average redshift of the SN search  $\langle z_{\text{SN}} \rangle$  (i.e. of the galaxy sample) is given by the average of the galaxy redshifts weighted by the effective control time:

$$\langle z_{\text{SN}} \rangle = \frac{\sum_{i=1}^N z_i \overline{CT}_i^{\text{SN}}}{\sum_{i=1}^N \overline{CT}_i^{\text{SN}}} \quad (4)$$

where  $N$  is the number of galaxies of the sample. It results that  $\langle z_{\text{Ia}} \rangle = 0.32$ ,  $\langle z_{\text{cc}} \rangle = 0.26$  for Ia and CC SNe respectively. The lower  $\langle z \rangle$  for CC SNe is obviously due to the fact that, on average, these are intrinsically fainter than Ia.

Considering that we have a sample of galaxies with a wide spread in redshift, to derive an estimate of the SN rates we have computed the expected SN counts as a function of redshift, derived by summing the contribution of individual SN types and using different assumptions for the rate evolution with redshift. For the latter we assume a power law dependence  $r_{\text{SN}}(z) = r_{\text{SN}}^0(1+z)^\alpha$ , where  $r_{\text{SN}}^0$  represent the local ( $z = 0$ ) rate for a given SN type and  $\alpha$  is the evolution index ( $\alpha = 0$  indicates no evolution). Using this model, the SN rate evolution parameters can be derived from the best fit between the expected and observed redshift distributions.

In practice, we derive the total expected SN detection  $N^{\text{exp}}(z)$  as the sum of the expected number of Ia and CC events:

$$N^{\text{exp}}(z) = N_{\text{Ia}}^{\text{exp}}(z) + N_{\text{cc}}^{\text{exp}}(z) \quad (5)$$

The expected redshift distributions of type Ia and CC SNe are given by:

$$N_{\text{Ia}}^{\text{exp}}(z) = \sum_{i=1}^n r_{\text{Ia}}^0 (1+z)^{\alpha_{\text{Ia}}-1} \overline{CT}_i^{\text{Ia}}(z) \quad (6)$$

$$N_{\text{cc}}^{\text{exp}}(z) = \sum_{i=1}^n r_{\text{cc}}^0 (1+z)^{\alpha_{\text{cc}}-1} \overline{CT}_i^{\text{cc}}(z) \quad (7)$$

where the sums are extended over the  $n$  galaxies in a given redshift bin  $z$  and the effective control time for core collapse SNe is computed as follows:

$$\overline{CT}_i^{\text{cc}}(z) = f_{\text{Ib/c}} \overline{CT}_i^{\text{Ib/c}}(z) + f_{\text{II}} \overline{CT}_i^{\text{II}}(z) \quad (8)$$

where we introduced the relative rates of type II,  $f_{\text{II}} = r_{\text{II}}^0/r_{\text{cc}}^0$  and type Ib/c,  $f_{\text{Ib/c}} = 1 - f_{\text{II}}$ . Here we make the

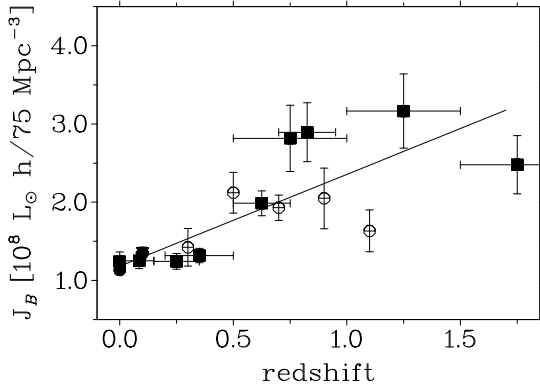


**Fig. 4.** Galaxy luminosity density ad different redshifts. Data are from (Madau, Pozzetti, & Dickinson 1998; Wolf et al. 2003; Blanton et al. 2003; Norberg et al. 2002). The line represents the best fit using a  $(1+z)^\alpha$  power law (see the text for details).

further assumption that the relative rates of different CC types do not change with redshift and are equal to the local ones, i.e.  $f_{II} = 0.8$ . (Cappellaro et al. 1999).

As a first step, we have tested the null hypothesis that the SN rates per unit blue luminosity do not change with redshift ( $\alpha_{Ia} = \alpha_{cc} = 0$ ) and they are equal to the local values, namely  $r_{Ia}^0 = 0.20 \pm 0.05 [h^2 \text{SNu}]^4$  and  $r_{cc}^0 = 0.47 \pm 0.19 [h^2 \text{SNu}]$  (Cappellaro et al. 1999). Under this hypothesis, in our galaxy sample one would expect 13.2 events, which is significantly smaller than the 28.2 actually observed. This already points out that the global SN rate must increase rapidly with redshift.

In our case, since we do not have the spectroscopic classification for all the SN candidates, we cannot directly use equation (3) to derive individual SN rates. Unfortunately, with the limited statistics available to date and the incomplete spectroscopic classification, we cannot determine rates and evolutions of both SN Ia and CC SNe from our data alone and we need to use other data sets. For this purpose we have exploited the published measurements of SN Ia rate at different redshifts (Blanc et al. 2004; Madgwick et al. 2003; Hardin et al. 2000; Pain et al. 2002; Tonry et al. 2003) to fix the evolution of SN Ia and to derive the CC rate.

One further complication is that some of the high redshift SN Ia measurements were given only per unit volume (Madgwick et al. 2003; Pain et al. 2002; Tonry et al. 2003). To convert these numbers into rate per unit luminosity (SNu scale), we need consistent estimates of the luminosity density at different redshift. For this purpose we collected from the literature recent measurements of the  $B$  luminosity density for the redshift range relevant for our SN search (Fig. 4). As can be seen, the measurements show a relatively high dispersion, particularly large at high

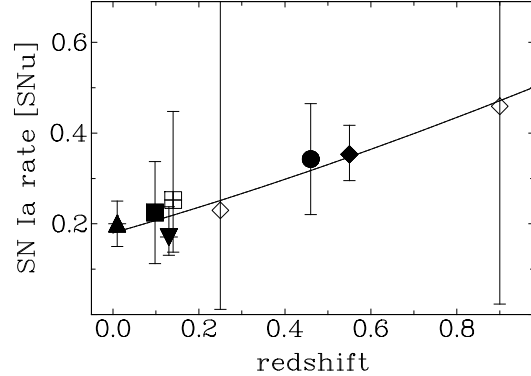


**Fig. 5.** Measurements of the SN Ia rate at different redshifts. References are as follows: filled triangle - (Cappellaro et al. 1999), filled upside-down triangle - (Blanc et al. 2004), filled square - (Madgwick et al. 2003), empty square - (Hardin et al. 2000), filled circle - (Tonry et al. 2003), filled diamond - (Pain et al. 2002), empty diamond - (Gal-Yam, Maoz, & Sharon 2002). The line is a fit with the power law in  $(1+z)$  (see the text for details). Because of the large errorbars the Gal-Yam et al. estimates have not be used for the fit.

redshift. The best fit with a power law  $\rho = \rho_0(1+z)^{\alpha_\rho}$  gives  $\rho_0 = 1.18 \times 10^8 [h L_{B\odot} \text{Mpc}^{-3}]$  and  $\alpha_\rho = 1.0$ . This has been used, in particular, to convert the rate per unit volume of Pain et al. (2002) and Tonry et al. (2003).

The published values of the SN Ia rate (in SNu) are plotted in Fig. 5, which convincingly shows a redshift evolution. This can be fitted with a power law relation with  $r_{Ia}^0 = 0.18 \pm 0.04 h^2 \text{SNu}$  and  $\alpha_{Ia} = 1.5 \pm 0.6$ .

Assuming that the SN Ia rate evolution is known, we can use the observed SN counts to constrain the evolution of core collapse rates. To this end, it is convenient to rewrite eq. (7) as follows:

$$N_{cc}^{\text{exp}}(z) = \sum_{i=1}^n r_{cc}^{\langle z_{cc} \rangle} \frac{(1+z)^{\alpha_{cc}-1}}{(1+\langle z_{cc} \rangle)^{\alpha_{cc}}} \overline{CT}_i^{cc}(z) \quad (9)$$

which is referring the rate to the average redshift  $\langle z_{cc} \rangle = 0.26$  in our case of the galaxy sample.

By means of a maximum-likelihood method we search for the values of  $r_{cc}^{\langle z_{cc} \rangle}$  and  $\alpha_{cc}$  which give the best fit between observed and expected distributions as a function of redshift. Resulting confidence levels are shown in Fig. 6. We found that  $r_{cc}(z = 0.26) = 1.45_{-0.45}^{+0.55} h^2 \text{SNu}$  and  $\alpha_{cc} = 2.9_{-2.9}^{+2.9}$  where the quoted errors are the  $1-\sigma$  confidence level. Clearly the parameter  $\alpha_{cc}$  describing the CC-rate evolution is poorly confined by our data alone, but the fair agreement with the measurement in the local Universe (cf. Fig. 8) is comforting.

The comparison between the observed and expected distribution for the best fit parameters is shown in Fig. 7. We notice that in our search about 2/3 of the observed

<sup>4</sup> 1 SNu = 1 supernova century<sup>-1</sup>  $10^{-10} L_{B\odot}$ .

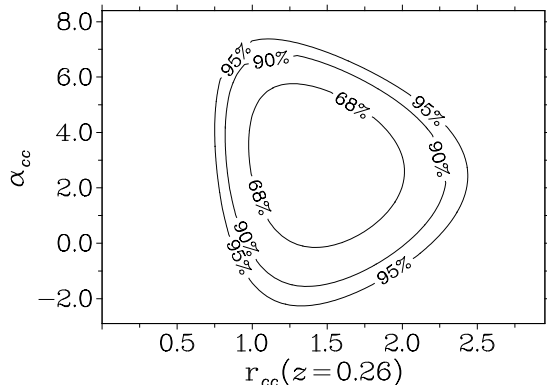


**Fig. 6.** Confidence level for the maximum-likelihood test.

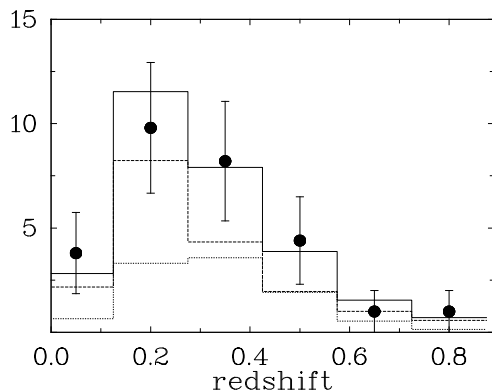


**Fig. 7.** Observed (points with statistical errorbars) and expected (solid line) redshift distribution of SN counts. The short-dashed and long-dashed lines are the expected type Ia and CC SN counts respectively.

SNe are expected to be CC and only 1/3 SN Ia. This is consistent with what we have found when spectroscopic confirmation was available (cf. Table 3).

The conclusion is that the CC SN rate at  $\langle z \rangle \sim 0.3$  appears to be a factor 3 higher than in the local Universe.

## 6. Uncertainties

The errors quoted before for the rate and evolutionary index parameter are purely statistical. Even though they are large, systematic errors need also to be considered. Indeed, although we made our best to exploit the significant observational effort, this first estimate of the CC rate at  $z > 0$  should be regarded as preliminary in many respects. In the following we highlight what we believe are the most severe caveats. Note that we will not discuss here systematics which originate from the uncertainties on the SN properties (absolute magnitudes, light curves, intrinsic dispersion). For them, in fact, we have made the same assumptions as for the computation of local rates

(Cappellaro et al. 1999) and therefore they are expected to cancel out in the comparison. Also we do not address the uncertainties in the cosmological model which was adopted and we rather focus on other aspects.

As we mentioned above, the most severe concern is the lack of spectroscopic classification for all candidates. In particular, we had to account in a statistical manner for the expected contamination by AGNs, assigning a weight of 0.4 to the candidates coinciding with the host galaxy nucleus. In order to evaluate the impact of this assumption, we have computed the best fit for two extreme cases: *a*) all nuclear candidates are AGNs or *b*) 80% of the nuclear candidates are indeed SNe. The two extreme cases encompass the ranges:  $r_{cc}^{(z_{cc})} = 1.3 \div 1.9 h^2 \text{ SNU}$  and  $\alpha_{cc} = 3.4 \div 2.3$  for the two fit parameters respectively. Therefore although important, this uncertainty is not likely to affect our conclusions.

Another concern is related to the limited accuracy in the characterization of the galaxy sample through photometric redshifts, due to the poor sampling of the galaxy SEDs. To check the possible influence of this uncertainty, for the 1375 galaxies of the AXAF field which we have in common with the COMBO17 surveys we computed the expected number of events alternatively using our own estimates for the galaxy redshifts and those reported in Wolf et al. (2003). We found that to match the SN number count in the AXAF field, using as reference the COMBO17 redshift estimates the rate  $r_{cc}^{(z_{cc})}$  has to be higher by  $\sim 10\%$  compared with our own redshift estimates. This is a small difference which is completely hidden by the statistical errors.

Of more concern is that in the current work we did not attempt to correct for the bias due to extinction in the host galaxies. This applies to all other estimates of SN rates at high redshift published so far. It is well known that in local SN searches there is a severe bias for SN detection in spiral galaxies which are not observed face-on (Cappellaro et al. 1999). This is attributed to the concentration of dust in the plane of the spiral galaxy disk which causes a higher average extinction for the inclined ones. Because of the wavelength dependence of extinction, it is expected that the blue photographic surveys which were used to derive the estimates of the local rates are heavily affected. For the same reason, it is sometimes claimed that CCD searches in nearby galaxies do not need to be corrected. This cannot be entirely true because the bias is seen even in the list of events discovered in the last few years mainly by CCD SN searches (Cappellaro et al. 2004). But even if we accept this claim, we stress that if high redshift galaxies have the same dust content as local ones then, just because of redshift, host galaxy extinction should cause a similar bias for blue band searches in nearby galaxies as for red searches in high redshift galaxies. Unfortunately, current data on high redshift SN searches do not allow to measure the size of this bias.

At the moment, we can only add that any correction is likely to increase, possibly even significantly, the CC

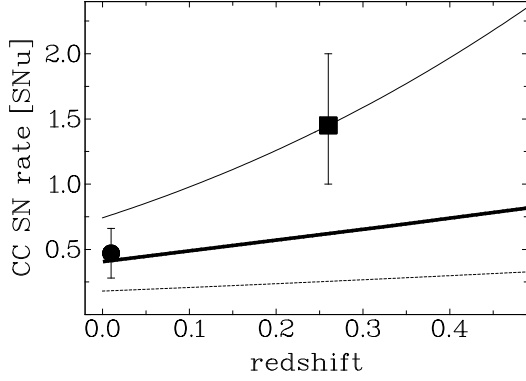


**Fig. 8.** CC SN rate with redshift. **The dot is the estimate of the local CC SN rate from Cappellaro et al. (1999) whereas the square is the new measurement derived in this paper.** The solid line shows the deduced evolution with redshift. The dashed line shows the deduced type Ia rate evolution (see the text for details). The thick solid line is the CC SN rate evolution predicted by model M2 of Sadat et al. (1998).

estimate reported here. In summary none of the reported uncertainties, even if important, seems to undermine the main conclusion reached here, that a significant evolution of the CC rate must be present even for this small look back time.

## 7. Discussion

When we compare our result with the models we find that, in the redshift range we are exploring, the current predictions indicate a much shallower evolution of the CC rate (Sadat et al. 1998; Madau et al. 1998; Calura & Matteucci 2003; Kobayashi et al. 2000) than actually observed.

As an example, in Fig.8 we show the predictions of Sadat et al. (1998) in the most favorable case (model M2 which corresponds to a higher SFR at high redshift). Although at a  $2\text{-}\sigma$  level the model is consistent with our measurement, we remark that taken to face value the observed rate at  $z=0.26$  is a factor 2 higher than the model. This becomes even more significant if we consider that, due to the lack of extinction correction, our estimate is expected to be a lower limit to the actual CC rate.

On the other hand, the CC rate evolution is directly related to the adopted history of SFR for which there are many new estimates. Indeed, considering the short evolutionary time scale of the CC SNe progenitors ( $< 5 \times 10^7$  yr) and under the assumption that the initial mass function (IMF) and the mass range of the CC progenitors do not change significantly in the redshift range of interest,

there is a simple direct relation between the SFR and the CC rate, namely:

$$r_{cc} = \psi \frac{\int_{M_l^{cc}}^{M_u^{cc}} \phi(\mathcal{M}) d\mathcal{M}}{\int_{M_L}^{M_U} \mathcal{M} \phi(\mathcal{M}) d\mathcal{M}} \quad (10)$$

where  $\psi$  is the SFR at the given redshift,  $\phi(\mathcal{M})$  is the IMF,  $M_L - M_U$  is the mass range of the IMF and  $M_l^{cc} - M_u^{cc}$  the mass range for the CC SN progenitors. In particular, adopting a Salpeter IMF in the range  $M_L = 0.1$  to  $M_U = 125 M_\odot$  and  $M_l^{cc} = 8$ ,  $M_u^{cc} = 50 M_\odot$  for the lower and upper limits of the mass of CC SN progenitors we derive  $r_{cc} \simeq 0.007\psi$ .

Usually the cosmic SFR is reported per unit of comoving volume and hence, for the comparison with SN rate evolution, it is convenient to translate the latter to the same unit using the known evolution of the luminosity density (Fig. 4). With this conversion, the CC SN rate per unit volume results  $r_{cc}^V(z = 0.26) = 2.2_{-0.7}^{+0.8} \times 10^{-4} h^3 \text{yr}^{-1} \text{Mpc}^{-3}$  (whereas the local value translates in  $r_{cc}^V(z = 0) = 5.5 \pm 2.2 \times 10^{-5} h^3 \text{yr}^{-1} \text{Mpc}^{-3}$ ). Finally, using eq. 10, we converted the CC rate in SFR, obtaining  $\psi(z = 0.26) = 3.1_{-1.0}^{+1.1} \times 10^{-2} h^3 M_\odot \text{yr}^{-1} \text{Mpc}^{-3}$  (and  $\psi(z = 0) = 7.9 \pm 3.1 \times 10^{-3} h^3 M_\odot \text{yr}^{-1} \text{Mpc}^{-3}$  for the local value).

Recently, Fujita et al. (2003) have published an estimate of the SFR based on the  $H\alpha$  luminosity density at  $z \simeq 0.24$ . This is shown in Fig.9 where are also reported other estimates of the SFR at different redshifts (adapted from Fujita et al. (2003), see references therein). As noted by Fujita et al. (2003) there is a systematic difference in the SFR deduced from the  $H\alpha$  luminosity density (filled symbols) compared with that derived from the UV luminosity density non corrected for extinction (empty symbols), with the former being significantly smaller at all redshift. However, it has been shown that this disagreement can be removed with a proper extinction correction (Rosa-González et al. 2002; Hippelein et al. 2003).

As seen in Fig. 9, our measurement is in excellent agreement with the value of Fujita et al. (2003) and in general with the rapid SFR evolution deduced from  $H\alpha$  luminosity density. Our conclusion, from the evolution of the core collapse SN rate is that at a redshift  $z = 0.26$ , that is at a look back time of 2.8 Gyr with the adopted cosmology, the SFR per unit comoving volume was three times higher than in local Universe. **We stress again that, because our measurement of the CC SN rate is not corrected for extinction, this is likely to be a lower limit (cf Sect. 6).**<sup>5</sup>

<sup>5</sup> After submission of this article, two preprints have been posted reporting new estimates of the SN rate evolution up to redshift 1.6, as part of the Great Observatories Origins Deep Survey (Strolger et al. 2004; Dahlsen et al. 2004). The main caveat is that, like in our case, they could obtain spectroscopic classification only for a fraction of the candidates. In any case, it turns out that their estimate of the CC SN rate

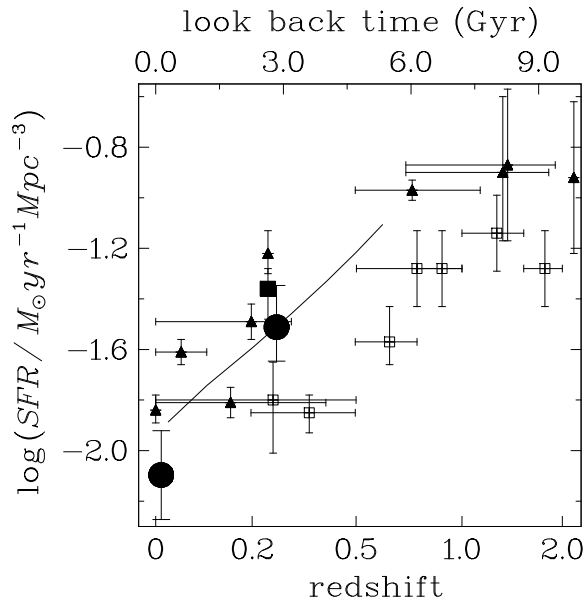


**Fig. 9.** We compare our estimate of the SFR at redshift  $z = 0.26$  (big filled dot) with the recent estimate of Fujita et al. (2003) based on the  $H\alpha$  luminosity density at  $z = 0.24$  (filled square). Also shown are estimates of the SFR at other redshifts based either on measurements of the  $H\alpha$  (filled symbols) or of the UV luminosity density (adapted from Fujita et al. (2003) and reference therein). Also plotted is the value derived from the local CC rate (also big filled dot).

*Acknowledgements.* We like to thank Michele Massarotti for the advices on the photometric redshift technique. This research has made use of the NASA/IPAC Extragalactic Database (NED) which is operated by the Jet Propulsion Laboratory, California Institute of Technology, under contract with the National Aeronautics and Space Administration. AC acknowledges support from CONICYT, Chile, through grant FONDECYT 1000524. SV acknowledges support from the program “Promozione della ricerca scientifica Regione Campania”, Legge Regionale n. 5 del 28/03/2002.

## References

- Alard, C. 2000, *A&AS*, 144, 363  
 Arnouts, S., Vandame, B., Benoist, C., et al. 2001, *A&A*, 379, 740  
 Bertin, E. & Arnouts, S. 1996, *A&AS*, 117, 393  
 Blanc, G., et al. 2004, in preparation  
 Blanton, M. R., Hogg, D. W., Bahcall, N. A., et al. 2003, *ApJ*, 592, 819  
 Bolzonella, M., Miralles, J.-M., & Pelló, R. 2000, *A&A*, 363, 476  
 Branch, D., Livio, M., Yungelson, L. R., Boffi, F. R., & Baron, E. 1995, *PASP*, 107, 1019

at redshift  $z=0.3$  is in remarkable agreement with the result reported here.

- Bruzual A., G. & Charlot, S. 1993, *ApJ*, 405, 538  
 Calura, F., Matteucci, F., 2003, *ApJ* 596, 734  
 Cappellaro, E., Turatto, M., Benetti, S., Tsvetkov, D. Y., Bartunov, O. S., & Makarova, I. N. 1993, *A&A*, 273, 383  
 Cappellaro, E., Turatto, M., Tsvetkov, D. Y., Bartunov, O. S., Pollas, C., Evans, R., & Hamuy, M. 1997, *A&A*, 322, 431  
 Cappellaro, E., Evans, R., & Turatto, M. 1999, *A&A*, 351, 459  
 Cappellaro, E., Barbon, R., & Turatto, M. 2004, IAU Colloquium 192 “Supernovae (10 years of SN 1993J)”, Valencia, Spain, eds. J. M. Marcaide and K. W. Weiler, in press  
 Coleman, G. D., Wu, C.-C., & Weedman, D. W. 1980, *ApJS*, 43, 393  
 Dahlén, T. & Fransson, C. 1999, *A&A*, 350, 349  
 Dahlén, T., Strolger, L.-G., Riess, A.G., et al., *ApJin* press (astro-ph/0404547)  
 Fujita, S. S., Ajiki, M., Shioya, Y., et al. 2003, *ApJ*, 586, L115  
 Gal-Yam, A., Maoz, D., & Sharon, K. 2002, *MNRAS*, 332, 37  
 Hardin, D., Afonso, C., Alard, C., et al. 2000, *A&A*, 362, 419  
 Heger, A., Fryer, C. L., Woosley, S. E., Langer, N., & Hartmann, D. H. 2003, *ApJ*, 591, 288  
 Hippelein, H., Maier, C., Meisenheimer, K., et al. 2003, *A&A*, 402, 65  
 Kobayashi, C., Tsujimoto, T., & Nomoto, K. 2000, *ApJ*, 539, 26  
 Landolt, A. U. 1992, *AJ*, 104, 340  
 Madau, P., Della Valle, M., & Panagia, N. 1998, *MNRAS*, 297, L17  
 Madau, P., Pozzetti, L., & Dickinson, M. 1998, *ApJ*, 498, 106  
 Madgwick, D. S., Hewett, P. C., Mortlock, D. J., & Wang, L. 2003, *ApJ*, 599, L33  
 Norberg, P., Cole, S., Baugh, C. M., et al. 2002, *MNRAS*, 336, 907  
 Pain, R., Hook, I. M., Deustua, S., et al. 1996, *ApJ*, 473, 356  
 Pain, R., Fabbro, S., Sullivan, M., et al. 2002, *ApJ*, 577, 120  
 Riello, M., Altavilla, G., Cappellaro, E., et al. 2003, From Twilight to Highlight: The Physics of Supernovae. Proceedings of the ESO/MPA/MPE Workshop held in Garching, Germany, 29-31 July 2002, p. 400., 400  
 Riello, M. 2003, *Mem. SAI*, 74, 984  
 Rosa-González, D., Terlevich, E., & Terlevich, R. 2002, *MNRAS*, 332, 283  
 Sadat, R., Blanchard, A., Guideroni, B., & Silk, J. 1998, *A&A*, 331, L69  
 Schechter, P. 1976, *ApJ*, 203, 297  
 Schmidt, B. P., Suntzeff, N. B., Phillips, M. M., et al. 1998, *ApJ*, 507, 46

- Strolger, L.-G., Riess, A.G.,Dahlén, T., et al., ApJin press  
(astro-ph/0404546)
- Sullivan, M., Ellis, R., Nugent, P., Smail, I., & Madau, P.  
2000, MNRAS, 319, 549
- Tonry, J. L., Schmidt, B. P., Barris, B., et al. 2003, ApJ,  
594, 1
- Valdes, F. G. 1998, ASP Conf. Ser. 145: Astronomical  
Data Analysis Software and Systems VII, 7, 53
- Yungelson, L. R. & Livio, M. 2000, ApJ, 528, 108
- Wolf, C., Meisenheimer, K., Rix, H.-W., Borch, A., Dye,  
S., & Kleinheinrich, M. 2003, A&A, 401, 73